



RESEARCH ARTICLE https://doi.org/10.1158/2767-9764.CRC-23-0431

**OPEN ACCESS** 

# **Small Extracellular Vesicles Promote** Stiffness-mediated Metastasis





## **ABSTRACT**

Tissue stiffness is a critical prognostic factor in breast cancer and is associated with metastatic progression. Here we show an alternative and complementary hypothesis of tumor progression whereby physiologic matrix stiffness affects the quantity and protein cargo of small extracellular vesicles (EV) produced by cancer cells, which in turn aid cancer cell dissemination. Primary patient breast tissue released by cancer cells on matrices that model human breast tumors (25 kPa; stiff EVs) feature increased adhesion molecule presentation (ITG $\alpha_2\beta_1$ , ITG $\alpha_6\beta_4$ , ITG $\alpha_6\beta_1$ , CD44) compared with EVs from softer normal tissue (0.5 kPa; soft EVs), which facilitates their binding to extracellular matrix proteins including

nation. Moreover, normal, resident lung fibroblasts treated with stiff and soft EVs change their gene expression profiles to adopt a cancer-associated fibroblast phenotype. These findings show that EV quantity, cargo, and function depend heavily on the mechanical properties of the extracellular microenvironment.

collagen IV, and a 3-fold increase in homing ability to distant organs in

mice. In a zebrafish xenograft model, stiff EVs aid cancer cell dissemi-

Significance: Here we show that the quantity, cargo, and function of breast cancer-derived EVs vary with mechanical properties of the extracellular microenvironment.

## Introduction

The extracellular matrix (ECM), a network of acellular components predominantly made of collagen, controls tissue structure, modulates cell adhesion and dissemination, influences the secretome, and conveys mechanical signals (1-4). Tissues inherently have unique structures and stiffnesses that lend to specific biological processes (5-8). An increase in ECM stiffness often correlates with poor prognosis in solid tumors (9-14), explained in part by stiffness-mediated enhanced cancer cell migration and proliferation at the primary tumor (15-18). As tumors develop, the density and composition of the ECM changes (19). Because of chronic inflammation, often fibrotic tissue forms at and around

the tumor site (20-22). The increased cross-linking of the ECM can lead to leaky vasculature and promote intravasation (23-26). Cellular phenotypes also change to promote tumor progression, that is, fibroblasts develop a cancerassociated phenotype that increases the deposition of fibrillar collagen and protumorigenic signaling (27, 28). Despite knowing the mechanical complexities of tumor growth and metastasis, cancer research and the development of therapeutics rely heavily on static model systems, such as tissue culture plastic, that do not incorporate physiologically relevant parameters (29, 30).

Because of their discovery, extracellular vesicles (EV) have primarily been collected and analyzed from tumor cells grown on tissue culture-treated plastic

Hopkins Bayview Medical Center, Baltimore, Maryland. <sup>9</sup>Department of Oncology, Johns Hopkins School of Medicine, Baltimore, Maryland.

A. Sneider, Y. Liu, and B. Starich contributed as co-first authors to this article. Current address for R. Vij: Leibniz Institute for Natural Product Research and Infection Biology, Hans-Knöll-Institute, Jena, Germany.

Corresponding Authors: Denis Wirtz, Johns Hopkins University, 3400 N. Charles St., Baltimore, MD 21218. E-mail: wirtz@jhu.edu; and T.S. Karin Eisinger-Mathason, University of Pennsylvania, 421 Curie Blvd, Philadelphia, PA 19104. E-mail: karineis@pennmedicine.upenn.edu

doi: 10.1158/2767-9764.CRC-23-0431

This open access article is distributed under the Creative Commons Attribution 4.0 International (CC BY 4.0) license.

© 2024 The Authors; Published by the American Association for Cancer Research

<sup>1</sup>Department of Chemical and Biomolecular Engineering, Johns Hopkins Physical Sciences-Oncology Center and Institute for NanoBioTechnology, Johns Hopkins University, Baltimore, Maryland. <sup>2</sup>Abramson Family Cancer Research Institute, Department of Pathology and Laboratory Medicine, Penn Sarcoma Program, University of Pennsylvania Perelman School of Medicine, Philadelphia, Pennsylvania. <sup>3</sup> Johns Hopkins Institute for NanoBioTechnology, Johns Hopkins University, Baltimore, Maryland. <sup>4</sup>Department of Materials Science and Engineering and Institute for NanoBioTechnology, Johns Hopkins University, Baltimore, Maryland. <sup>5</sup>W. Harry Feinstone Department of Molecular Microbiology and Immunology, Johns Hopkins University Bloomberg School of Public Health, Baltimore, Maryland. <sup>6</sup>Bioengineering and Aerospace Engineering Department, Universidad Carlos III de Madrid, Leganés, Spain. <sup>7</sup>Instituto de Investigación Sanitaria Gregorio Marañón, Madrid, Spain. <sup>8</sup> Johns Hopkins Breast Center, Johns

ware (31). Until recently, the physiologic relevance of EVs obtained in this manner remained largely unknown. Now EVs are a diverse group of lipid bilayer encapsulated particles secreted by cells that display and encapsulate functional proteins and nucleic acids (32, 33). Small EVs, particularly exosomes that are between 30 and 150 nm in diameter, have shown great promise as biomarkers and therapeutic agents for the treatment of disease (31, 34-37). Because of their size, exosomes have the potential to disseminate great distances from their site of secretion (38, 39). Small EVs can transfer their cargo to other cell types and influence homeostasis and disease progression (36, 40-46). Cancer-derived exosomes can increase vascular leakiness, reprogram bone marrow progenitors, increase tumor growth and metastasis (47), facilitate premetastatic niche formation (48-50), more effectively fuse with target cells (51); and aid in evading immune detection (31, 52). The role of tissue stiffness on EV secretion and metastasis remains largely unexplored (53, 54). Therefore, we sought to characterize the importance of physiologically relevant physical tissue properties (e.g., stiffness) in EV-mediated metastatic dissemination.

Herein we explore how modulating stiffness in the tumor microenvironment can influence cancer progression through EVs. We observed in primary patient tissues that more EVs are secreted from stiff tissue than softer tissue. We investigated exosomes isolated from breast cancer cells cultured on plastic (~3 GPa), 25 kPa (breast tumor stiffness, stiff), and 0.5 kPa (normal tissue stiffness, soft) substrates. EVs from cells on substrates at tumor tissue stiffness have different cargo than those vesicles from soft and plastic substrates. The stiff EV cargo is enriched in integrins (ITG $\alpha_2\beta_1$ , ITG $\alpha_6\beta_4$ , ITG $\alpha_6\beta_1$ ), adhesion proteins (CD44), and immune evasion signals over the soft and plastic EVs. These stiff EVs are better able to reach and be retained in distant tissues in vivo in mice and adhere to specific ECM proteins like collagen IV. In addition, stiff EVs promote cancer cell dissemination in vivo in zebrafish over soft EVs. EVs isolated from cells cultured on plastic do not consistently match either the physiologic stiff or soft conditions. Once cancer cells have arrived in distant tissues, the cells experience the mechanically soft environment of normal tissue. While stiff EVs appear to downregulate immune signaling from resident fibroblasts in the lung via a decrease in expression in S100A4, S100A6, S100A12, and S100A13 to potentially to aid cancer cells in evading immune detection, the soft EVs demonstrate the ability to upregulate expression of cancer-associated fibroblast (CAF) markers (ACTA2, COL1A1, VIM) while also presenting increased inflammatory capacity (elevated S100A10, S100A16) in the resident fibroblasts. These results suggest that matrix stiffness influences vesicular secretion and cargo to aid cancer cells at different stages of the metastatic cascade.

# **Materials and Methods**

## **Cell Culture**

Human breast cancer cell lines MDA-MB-231 (RRID:CVCL\_0062, Female) and human pancreatic cancer cell line BxPC-3 (RRID:CVCL\_0186, Female) were obtained from ATCC. IMR-90 (RRID:CVCL\_0347, Female) human lung fibroblasts were provided as a generous gift from Daniele Gilkes (Johns Hopkins University, Baltimore, MD). Cell lines were authenticated by initial vendor certification; annual authentication was not performed. All cell lines were cultured in DMEM (Corning, catalog no. 10-0130-CV) containing 10% FBS (Corning, catalog no. 35-010-CV) and 1% penicillin-streptomycin (Gibco, catalog no. 15140122; refs. 55, 56). Cells were maintained at 37°C and 5% CO<sub>2</sub> and sustained in culture between passage 2 and 15. Cell lines were confirmed *Mycoplasma* negative using MycoAlert (Lonza, catalog no. LT07-318) every 6 months.

#### **EV Collection**

Prior to vesicle collection, cells were seeded at 70% confluency and cultured on 177 cm² 0.5 kPa Collagen Type I Coated Plates (Matrigen, catalog no. PS150-COL-0.5), 177 cm² 25 kPa Collagen Type I Coated Plates (Matrigen, catalog no. PS150-COL-25), and 150 cm² plastic tissue culture Falcon flasks ("plastic"; Corning, catalog no. 355001). After 24 hours incubation at 37°C, cells were washed with Dulbecco's phosphate buffered saline (DPBS, Corning, catalog no. 20-031-CV) and changed to DMEM containing 10% exosome-depleted FBS (Gibco, catalog no. A2720801) and 1% penicillin-streptomycin (Gibco, catalog no. 15140122). Following another 24 hours incubation at 37°C, EVs were collected and purified.

Cell culture supernatant was subjected to sequential centrifugation (800  $\times$  g for 5 minutes, 2,000  $\times$  g for 10 minutes, 10,000  $\times$  g for 30 minutes) at 4°C (Beckman Coulter Avanti J-E Centrifuge); filtered through a 0.22-µm PES filter (Genesee, catalog no. 25-244); and centrifuged twice at 100,000  $\times$  g for 2 hours at 4°C (Beckman Coulter Optima XE-90 Ultracentrifuge). Supernatant was replaced with DPBS between ultracentrifugation (UC) spins. The final vesicle pellet was resuspended in 1 mL DPBS. Samples were concentrated using a 2 mL 3 kDa Amicon filter (MilliporeSigma, catalog no. UFC200324). For the mouse experiments, samples were incubated with 1 µmol/L DiR dye (Thermo Fisher Scientific) prior to ultracentrifugation. For zebrafish and adhesion studies, EVs were labeled with the 7  $\mu$ mol/L CMTPX Dye (Thermo Fisher Scientific, catalog no. C34552) between ultracentrifugation steps. Free dye was pelleted at  $10,000 \times g$  (3  $\times$  10-minute spins) and EV containing supernatant ultracentrifuged and then concentration using Amicon. Protein concentration was determined using a Pierce bicinchoninic acid (BCA) protein assay kit (Thermo Fisher Scientific, catalog no. 23227) according to the manufacturer's protocol.

## **Size Distributions of EVs**

Size distribution and concentration of EVs were measured using a NanoSight NS300 (Malvern Preanalytical). Additional details are in the Supplementary Data

#### **Western Blot Analysis**

EV protein aliquots were lysed with 20%  $\beta$ -mercaptoethanol (Gibco, catalog no. 21985023) in 4X Laemmli buffer (Bio-Rad, catalog no. 1610747) for 5 minutes at 100°C. A total of 5  $\mu$ g of EV protein lysate determined by BCA was loaded per lane and separated by molecular weight on 4%–15% Mini-Protean Precast TGX Gels (Bio-Rad, catalog no. 4561086) and transferred to Trans-Blot Turbo Mini polyvinylidene difluoride membranes (Bio-Rad, catalog no. 1620261). Overnight incubation at 4°C with primary antibodies, including anti-TSG101 (1:500, Abcam, catalog no. ab125011, RRID: AB\_10974262) and anti-CD63 (1:1,000, Abcam, catalog no. ab193349, RRID: AB\_3095976) in 1X Tris-buffered saline, 0.1% Tween (TBST). Secondary antibody incubation with corresponding horseradish peroxidase–conjugated anti-rabbit (Cell Signaling Technology, catalog no. 7074, RRID:AB\_2099233) or anti-mouse secondary antibody (Cell Signaling Technology, catalog no. 7076, RRID:AB\_330924).

#### **Silver Stain**

Samples were prepared according to the Western blot protocol and run through a 4%–15% Mini-Protean Precast TGX Gel. The gels were then stained using the Pierce Silver Stain Kit (Thermo Fisher Scientific, catalog no. 24612) according to the manufacturer's protocol.

#### Transmission Electron Microscopy

A total of 10  $\mu$ L of sample was adsorbed to glow-discharged (EMS GloQube) 400 mesh ultra-thin carbon-coated grids (EMS CF400-CU-UL) for 2 minutes, followed by three quick rinses of TBS and stained with 1% UAT (uranyl acetate with 0.05% Tylose). Grids were immediately observed with a Philips CM120 at 80 kV and images captured with an AMT XR80 high-resolution (16-bit) 8 megapixel camera. Two biological repeats.

#### **Biodistribution of EVs in Mice**

All mouse work was performed following Johns Hopkins University and International Animal Care and Use Committee (IACUC) guidelines under animal protocol MO16A383. There was no statistical method to predetermine sample size. Six to 8 weeks old NCr nude (NCRNU-F sp/sp) females (Taconic) were each injected via tail vein with stained vesicles in DPBS at a quantity of 10  $\mu g$  of protein in 50  $\mu L$  per mouse (56). Twenty-four hours after injection, mice and their organs were imaged using the LI-COR Pearl Impulse Imaging System (LI-COR Biosciences). Images were analyzed in LI-COR Pearl Impulse Imaging System according to the manufacturer's instructions. The mean signal-to-noise ratio (SNR) was determined by subtracting the mean background intensity from the mean intensity of the region of interest (ROI) and dividing through by the SD of the background.

#### **Biodistribution of EVs and Cancer Cells in Zebrafish**

All procedures on zebrafish (Danio rerio) were approved by IACUC at The University of Pennsylvania (Philadelphia, PA). Fertilized zebrafish eggs of the transgenic strain expressing enhanced green fluorescent protein (EGFP) under the fli promoter (fli:EGFP) or mCherry under the flk promoter (flk:mCherry) were incubated at 28°C in E3 solution and raised using standard methods. Embryos were transferred to E3 solution containing 5  $\mu g/mL$  proteases and 0.2 mmol/L1-phenyl-2-thio-urea (Sigma) 24 hours postfertilization to dechorionate the fish embryos and prevent pigmentation, respectively. At 48 hours postfertilization, zebrafish embryos were anesthetized with 0.03% tricaine (Sigma) and then transferred to an injection plate made with 1.5% agarose gel for microinjection. Approximately 200,000 EVs suspended in PBS were injected into the perivitelline space of each embryo using a XenoWorks Digital Microinjector (Sutter Instrument). Each injection volume was between 5 and 10 nL. At 2-2.5 hours after the vesicle injection, 150 to 400 MDA-MB-231 cells labeled with NucBlue live cell stain ReadyProbe (Thermo Fisher Scientific, catalog no. R37605) and suspended in complete growth medium supplemented with 0.5 mmol/L Ethylenediaminetetraacetic acid (EDTA) were injected into the perivitelline space of each vesicle-bearing embryo. Pre-pulled micropipettes were used for the microinjection (Tip inner diameter [ID] 50 µm, base outer diameter [OD] 1 mm, Fivephoton Biochemicals). After injection, the fish embryos were immediately transferred to a PTU-E3 solution. Injected embryos were kept at 33°C and were examined every day to monitor tumor cell migration using a widefield microscope.

## Patient Tissue Sample Preparation for Mechanical Measurements

All patient tissue samples were obtained with written consent from the patient and approved by the Johns Hopkins Medicine Institutional Review Board. Tissue samples received from the patients were kept in 4°C DPBS immediately after mastectomy or lumpectomy. Tumor samples were then transferred for mechanical tests within 4 hours of resection. The tumor tissue was then sectioned to expose the ROIs for micromechanical mapping and compression tests.

#### **Tumor Stiffness Mapping Using Microindentation**

Dynamic indentation using a nanoindenter (Nanomechanics, Inc.) was used to characterize the tumor elastic modulus (57). Sneddon stiffness equation (58) was applied to relate dynamic stiffness of the contact to the elastic storage modulus of the samples (59, 60). Additional details are in the Supplementary Data document.

### **Compression Tests of Tumor-adjacent and Tumor Tissues**

Compression tests were performed as reported previously (61). Briefly, tissue samples were sectioned to obtain flat and parallel surfaces on all sides. Once the sample was sectioned, it was immediately staged on tensile/compression tester (MTS Criterion) for measurement (62). The top compression plate was lowered until in full contact with the tissue sample at minimal load. Once in contact, the samples could relax and stabilize for 1 minute before the actual compression test. Tissue samples were compressed at 0.25 mm/second deformation rate until 20% strain. Young modulus calculation was done on the best-fitted slope of the initial linear region ( $\sim$ 5%–10%) of the obtained stress-strain curve. A single measurement was obtained for each tissue.

# Vesicle Collection and Characterization for Patient Tissues

After mechanical measurements, tissue was transferred to 5 mL of 1% penicillin-streptomycin solution in 013-CV DMEM and incubated at 37°C overnight. After 24 hours, tissue was fixed in formalin and vesicles isolated from supernatant. Additional details are in the Supplementary Data document.

#### **ECM Binding Assay**

Substrates were obtained from Millicoat ECM Screening Kit (MilliporeSigma, catalog no. ECM205) and rehydrated according to manufacturer specifications. A total of 1.5  $\times$   $10^9$  CMTPX fluorescently labelled vesicles in 50  $\mu L$  DPBS (without Ca<sup>2+</sup> and Mg<sup>2+</sup>) were incubated on each substrate for 1 hour at 37°C. Wells were imaged at 10X TRITC channel with 100% light intensity and 100 ms exposure time (Nikon Eclipse Ti), and fluorescence was determined in ImageJ (RRID:SCR\_003070) via measuring the mean intensity of a fixed ROI. After removing the diluted suspension, the matrix was washed three times using DPBS (with Ca<sup>2+</sup> and Mg<sup>2+</sup>; Corning, catalog no. 20-030-CV) according to the manufacturer protocol and the wells were imaged again under DPBS (without  $Ca^{2+}$  and  $Mg^{2+}$ ) to minimize possible fluorescence deviation from ions. For all washing steps, slow manual pipetting was adopted to avoid disturbance of the adhered EV samples. Background intensity was determined from the negative control—PBS with CMTPX dye processed through the same ultracentrifugation and 3 kDa Amicon filtration steps as EV samples—and subtracted from sample intensity. Sample intensity postwash was divided by the prewash intensity values at same ROI to determine percentage of vesicles adhered to each substrate.

### **Fibroblast mRNA Expression Assay**

IMR-90 lung fibroblasts were seeded 2 days prior to the addition of vesicles. These cells were then washed with DPBS and incubated in exosome-depleted medium with vesicles or DPBS for 48 hours at 37°C. RNA was extracted according to manufacturer instructions for DirectZol Kit (Zymo Research, catalog no. R2050) after imaging (Nikon Eclipse Ti). cDNA was generated using iScript cDNA Kit (Bio-Rad, catalog no. 1708890) according to manufacturer instructions. Then qPCR was performed. Two biological repeats with three technical repeats per condition. Housekeeping gene value is a geometric mean

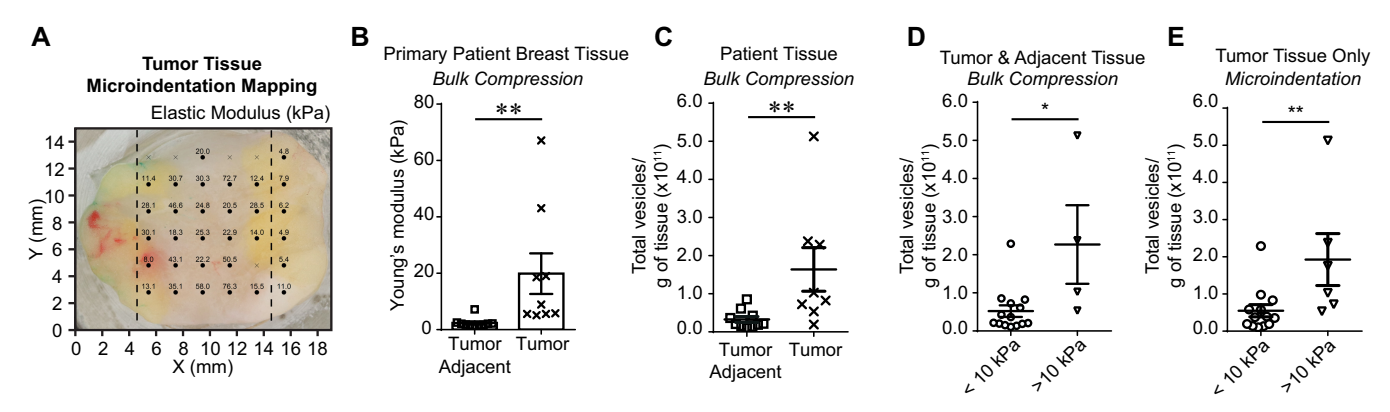


**FIGURE 1** Matrix stiffness impacts the quantity of EVs produced by patient tissue. **A,** Representative primary breast tumor tissue. Sample has been mechanically mapped using microindentation. Dark circles indicate measurements of the elastic modulus expressed in units of kPa. Crosses are nonmeasurable indentations. Dotted lines indicate where the tissue was sectioned into stiff (middle) and soft (right) regions for subsequent vesicle collection. **B,** Mean compression measurements (kPa, mean  $\pm$  SEM) of patient tumor and adjacent normal tissues. Ten adjacent normal tissue samples and nine tumor tissue samples. Nonparametric t test. **C,** Vesicles released per gram of tissue in pathologist determined tumor adjacent or tumor tissue patient samples. Ten normal tissue samples and eight tumor tissue samples. **D,** Combined tumor-adjacent and tumor tissues samples separated by mean compression measurements (kPa, mean  $\pm$  SEM). Fourteen samples < 10 kPa and four samples > 10 kPa. Nonparametric t test.

of  $\alpha$ -tubulin (*TUBA3C*), *GAPDH*, and TATA-Box Binding Protein (*TBP*). The primer sequences used are listed in Supplementary Table S1.

## **Quantifying EV Secretion**

To determine quantifiable variations, nanoparticle tracking analysis (NTA) particle concentrations were multiplied by UC sample volumes for a total particle number. Dividing the total vesicle number by the weight of the tissue provides a value of vesicles secreted per gram of tissue.

#### **EV Proteomics**

10-plex Tandem Mass Tag Proteomics (TMT Proteomics) performed on three biological replicates of EVs from cells cultured on tissue culture plastic, 25 kPa, and 0.5 kPa matrices (63). Data searched using SwissProt *Homo Sapiens* database with MASCOT in Proteome Discoverer 2.2 (RRID:SCR\_014477). Additional details are in the Supplementary Data document. The mass spectrometry proteomics data have been deposited to the ProteomeXchange Consortium via the PRIDE [1] partner repository with the dataset identifier PXD049019 and 10.6019/PXD049019.

#### **Statistical Analysis**

Statistical analysis was performed using Prism 6 (GraphPad Software, Inc.) to calculate the mean, SD, and SE mean. t test and one-way ANOVA were performed where appropriate to determine significance (GraphPad Prism, RRID:SCR\_002798). Biological and technical replicates are indicated throughout the figure captions. All graphical data are reported as mean  $\pm$  SEM. \*, P < 0.05; \*\*, P < 0.01; \*\*\*, P < 0.001; and \*\*\*, P < 0.0001.

## **Data Availability Statement**

The mass spectrometry proteomics data have been deposited to the ProteomeXchange Consortium via the PRIDE [1] partner repository with the dataset identifier PXD049019 and 10.6019/PXD049019. The datasets that support the findings of this study are available from the corresponding author upon request.

## Results

### Physiologically Relevant Tissue Stiffness Impacts EV Secretion in Patients

To determine physiologically relevant stiffnesses, we obtained primary patient breast tumor and adjacent normal tissues sectioned by a pathologist for mechanical measurements (Fig. 1A). Using a bulk compression test, a method that utilizes uniaxial compression, we found a statistically significant difference in the mean Young modulus of tumor tissues (19.9  $\pm$  7.1 kPa) and tumor adjacent tissues (2.4  $\pm$  0.5 kPa; Fig. 1B). In addition, tumor samples released significantly more vesicles per gram of tissue than tumor adjacent tissue (Fig. 1C; Supplementary Fig. S1A). Tumor tissue stiffness was further mapped using microindentation, a method that determines the local elastic modulus of evenly spaced points (Fig. 1A; Supplementary Fig. S1B). To investigate the effect of tumor stiffness on EVs, we separated the stiff sections (24.4  $\pm$  4.4 kPa, mean  $\pm$ SEM) and the soft sections (5.7  $\pm$  0.4 kPa) of the tumor tissues based on the microindentation results (Fig. 1D). We noted significant intratumoral and intertumoral heterogeneity, ranging from 2.9 to 76.0 kPa (Supplementary Fig. S1B). On the basis of these findings, we elected to use a 25 kPa matrix to represent stiffer human tumor tissue in our subsequent assays. Given our interest in investigating the impact of EVs at distant sites, such as the lung which has a stiffness ranging from 0.5 to 5 kPa (47, 64-69), we chose a matrix stiffness of 0.5 kPa to represent softer tissues. We compared EVs collected from cells grown on matrices at these physiologic stiffnesses to EVs derived from cells grown on plastic culture dishes with non-physiologic stiffness between 2 and

Following microindentation analysis of resected human breast cancer samples, we sectioned the tissues by stiffness and isolated EVs from stiff and soft regions. To preserve the integrity and micromechanics of these tissues, the tissues were not dissociated; therefore, isolated vesicles were released from both cancer and tumor-associated cells. Significantly more vesicles were released per gram of tissue with a mean tissue stiffness > 10 kPa than from tissues < 10 kPa (Fig. 1D and E; Supplementary Fig. SIA).

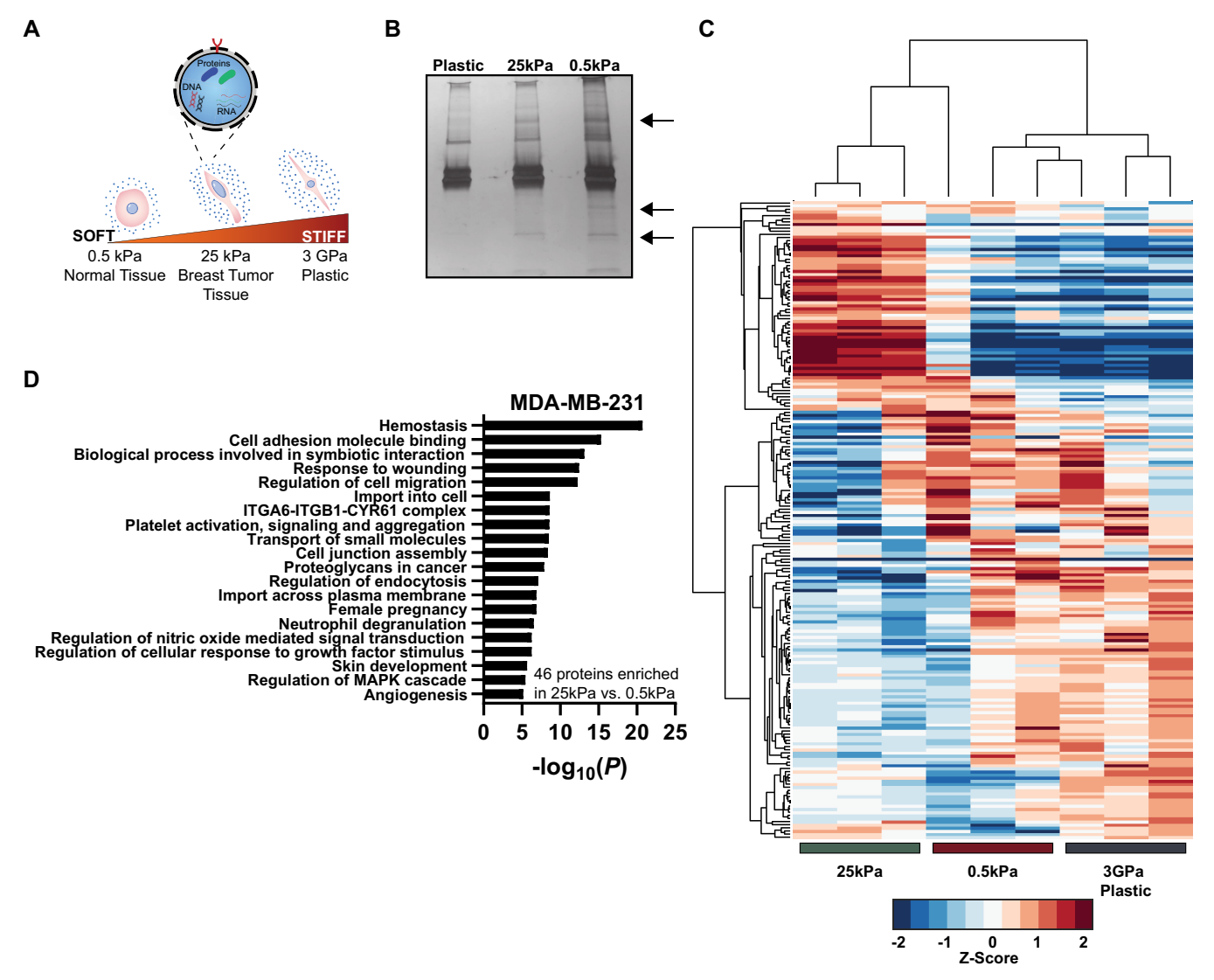


**FIGURE 2** EV cargo is affected by matrix stiffness. **A,** Schematic of EV secretion by cancer cells on standard plastic, tumor (25 kPa) stiffness and normal tissue (0.5 kPa) stiffness. **B,** Silver stain of EV isolated proteins. **C,** Clustergram of EV protein abundance values. The color scale corresponds to the log<sub>2</sub> normalized z-scored abundance values scaled to –2 and 2 for visual clarity. Three biological repeats. See also Supplementary Table S2. **D,** Gene ontology pathway analysis using Metascape for MDA-MB-231 EV proteins enriched in stiff EVs over soft EVs (79). Three biological repeats.

### **Matrix Stiffness Impacts EV Quantity and Protein Cargo**

Above, we determined that tissue stiffness impacts the quantity of vesicles released in breast tumors. Next, we investigated whether matrix stiffness affects EV morphology and protein cargo. Hereafter, we interchangeably refer to EVs released by cells on the plastic matrix as "plastic EVs," 25 kPa matrix as "stiff EVs," and 0.5 kPa matrix as "soft EVs." We compared plastic, stiff, and soft EVs derived from highly metastatic, triple-negative-breast cancer (TNBC) cell lines MDA-MB-231 as our primary model systems (Fig. 2A). We first verified that breast cancer cells displayed the expected stiffness-dependent morphology (18, 70), including a spindle shape on stiffer matrices and a round morphology on the soft matrix, prior to vesicle collection (Supplementary Fig. S2A).

The size of plastic, stiff, and soft EVs was determined using both NTA and transmission electron microscopy (TEM). NTA showed that the mean size of collected particles was between 100 and 150 nm for the TNBC and pancreatic

cancer cells across tested matrix stiffnesses (Supplementary Fig. S2B). Corroborating NTA, TEM indicated that plastic, stiff, and soft EVs showed the expected size and morphology of EVs (Supplementary Fig. S2C and S2D; refs. 71, 72). Analysis of the TEM images using a machine learning algorithm (73) confirmed that size and shape of EVs were independent of matrix stiffness (Supplementary Fig. S2D and S2E). Western blots of EV-specific markers (37, 74) confirmed that plastic, stiff, and soft EVs contained tetraspanin cluster of differentiation 63 (CD63) and tumor susceptibility gene 101 (TSG101) across all tested matrix stiffnesses (Supplementary Fig. S2F). While there were similarities in size and morphology, we found major differences in protein content of EVs produced by cancer cells on plastic, stiff, and soft matrices. We determined that there was a nonsignificant difference between the total number of vesicles and the amount of isolated protein between EV conditions (Supplementary Fig. S2G). We then loaded silver-stained electrophoresis gels based on total vesicular protein to normalize for changes in vesicle number and identified

qualitative protein cargo differences in the EVs as a function of overall matrix stiffness (Fig. 2B). To test the generality of these findings, we selected pancreatic cancer cell line BxPC3 given that an increase in stiffness is also linked to a poor prognosis in this disease, tumor progression is often characterized by significant changes in the ECM due to desmoplasia, and the selected physiologic stiffnesses also match that of normal tissue and extremely stiff tissue in the pancreas (18, 75–78). We find that the pancreatic cancer cells display the expected morphology on matrices of different stiffness (Supplementary Fig. S2A), the vesicle size and size distribution is independent of matrix stiffness (Supplementary Fig. S2B), the vesicles contain CD63 and TSG101 across all conditions (Supplementary Fig. S2F), and that proteins are differentially enriched in the BxPC3 EVs as a function of overall matrix stiffness (Supplementary Fig. S2H).

To quantify the observed variations in protein content in the breast cancerderived EVs, we performed mass spectrometry on plastic, stiff, and soft EVs (Fig. 2C; Supplementary Table S2). Proteomic analysis of the EVs identified over 200 proteins expressed in plastic, stiff, and soft EVs. Unsupervised clustering of normalized protein abundances revealed significant variations in content between the three conditions (Fig. 2C; Supplementary Table S2). Using an abundance ratio > 2-fold, we found only two proteins enriched in plastic-derived EVs over stiff EVs, while 52 proteins were enriched in stiff EVs over plastic EVs (Supplementary Fig. S3A). When comparing the physiologically relevant stiffnesses, three proteins were enriched in soft EVs over stiff EVs, and 46 proteins were enriched in stiff EVs over soft EVs (Supplementary Fig. S3B). In the final comparison, six proteins were enriched in plastic EVs relative to soft EVs, and nine enriched in soft EVs relative to plastic EVs (Supplementary Fig. S3C). Gene ontology analysis of proteins enriched in stiff EVs identified pathways related to the immune response, tumorigenesis, adhesion, and metastasis including response to wounding, ECM-receptor interaction, cell-junction organization, integrin complexes, and cellular response to IFN $\gamma$  and IL12 (Fig. 2D; Supplementary Fig. S3D; ref. 79).

The vesicle protein content indicates that plastic, stiff, and soft EVs may have different functional roles in promoting metastasis. Given that many of the pathways enhanced in the stiff over soft EVs overlapped with cell adhesion and cell–ECM interactions (Fig. 2D), we hypothesized that these matrix stiffness-dependent variations could impact EV biodistribution to different organs (lung, liver, etc.) and the ensuing spread of cancer cells from the primary tumor to these organs. Furthermore, we decided to focus herein on the stiff and soft EVs as the plastic EVs are less physiologically relevant, yielding different cargo that could impact functional assays.

#### Stiff EVs Show Enhanced Biodistribution In Vivo

To determine whether overall differences in molecular cargo, prompted by differing matrix stiffness, had a functional effect on the distribution and retention of breast cancer–derived EVs *in vivo*, we injected immunodeficient nude mice with fluorescent EVs via their tail veins (Fig. 3A). We chose a tail vein metastasis model, which forces metastasis to the lung, given our focus on near-infrared (NIR) from the dorsal, left, ventral, and right sides (Fig. 3B; Supplementary Fig. S4A). For all angles, the mean SNR was 2- to 3-fold greater for stiff EVs compared with soft EVs (Fig. 3C). In addition to lungs, we observed a 3-fold increase in the mean SNR for stiff EVs over soft EVs in primary filter organs—liver and spleen (Fig. 3D and E). Non-physiologic plastic EVs shared a similar biodistribution profile to 25 kPa (Supplementary Fig. S4A and S4B), with decreased retention in the liver (Supplementary Fig. S4C and S4D).

To identify the mechanism driving this stiffness-mediated EV biodistribution, we investigated whether the stiff and soft EVs bound differentially to ECM proteins, especially ECM molecules associated with tumor progression and metastasis (80, 81). Via quantification of total fluorescent signal, stiff EVs preferentially bound to collagen type IV relative to soft EVs (Fig. 3F). The stiff and soft EVs did not demonstrate significant differences in binding to collagen type I or laminin (Fig. 3F). On the basis of the enrichment of adhesion molecules in stiff EVs in the proteomics data, ITG $\alpha_2\beta_1$  and CD44 could facilitate the enhanced binding to collagen type IV (81–86, 87).

# Stiff EVs Promote Cancer Cell Dissemination and Survival *In Vivo*

Because breast cancer-derived stiff EVs were retained within common secondary sites to a much greater extent than soft EVs, and the stiff EVs bound preferentially to ECM proteins linked to metastasis, we sought to determine whether the EVs would directly affect cancer cell behavior during metastasis. To explore this scenario, we created a zebrafish xenograft model to explore cancer cell dissemination and survival *in vivo*. Zebrafish possess orthologs for 70% of human genes, are translucent allowing for real-time *in vivo* visualization, cost-effective, and lack adaptive immune systems during early embryogenesis, highlighting their utility as effective xenograft hosts. We utilize zebrafish embryos 2 days postfertilization (2 dpf).

PBS, breast cancer—derived stiff EVs, or breast cancer—derived soft EVs were injected into the yolk sac of zebrafish embryos 2 dpf, followed by injection of cancer cells within 2–2.5 hours of EV injection (Fig. 4A). Embryos were imaged at 24 hours to quantify cell dissemination (Fig. 4B and C). Quantification of embryos displaying cancer cell dissemination to the head and tail 24 hours after cell injection in a dye-only condition (no preinjected vesicles) showed that only 4.2% of fish exhibited a net transfer of cells out of the yolk sac to the head or tail of the fish (Fig. 4D). In contrast, 33.8% and 10.7% of fish preinjected with stiff and soft EVs, respectively, had disseminated cancer cells (Fig. 4D). Fish injected with plastic EVs had negligible dissemination (Supplementary Fig. S4E). These results suggest there is a role for EVs in mediating metastasis which depends critically on the physical properties of the microenvironment.

### **Soft EVs Transform Fibroblasts Into CAF-like Cells**

Because breast cancer—derived stiff EVs facilitate the dissemination of cancer cells (Fig. 4), we wanted to assess whether stiff and soft EVs would differentially affect the ability of cancer cells to form tumors at secondary sites by transforming resident stromal cells, particularly fibroblasts. Fibroblasts are responsible for maintaining homeostasis as immunoregulatory cells and through the generation of structural ECM molecules like collagen I (88–90). Because we observed the greatest differences in EV retention in the lungs, liver, and spleen, (Fig. 3E) and breast cancer frequently metastasizes to the lung *in vivo*, we assessed EV-mediated changes in the phenotype of normal lung fibroblasts (Fig. 5A and B). Cancer cells recruited to the lungs are exposed to a relatively soft microenvironment (0.5–1 kPa) at this distant site, which has a stiffness like that of normal breast tissues (91, 92).

To determine how the mechanically new environment of the lung may promote further tumor progression, we investigated how stiff and soft EVs differentially modulated resident lung fibroblasts by assessing the expression of a several CAF markers (27, 88–90, 93–97). Lung fibroblasts treated with stiff and soft EVs showed significantly different abilities to induce CAF-associated markers. Soft

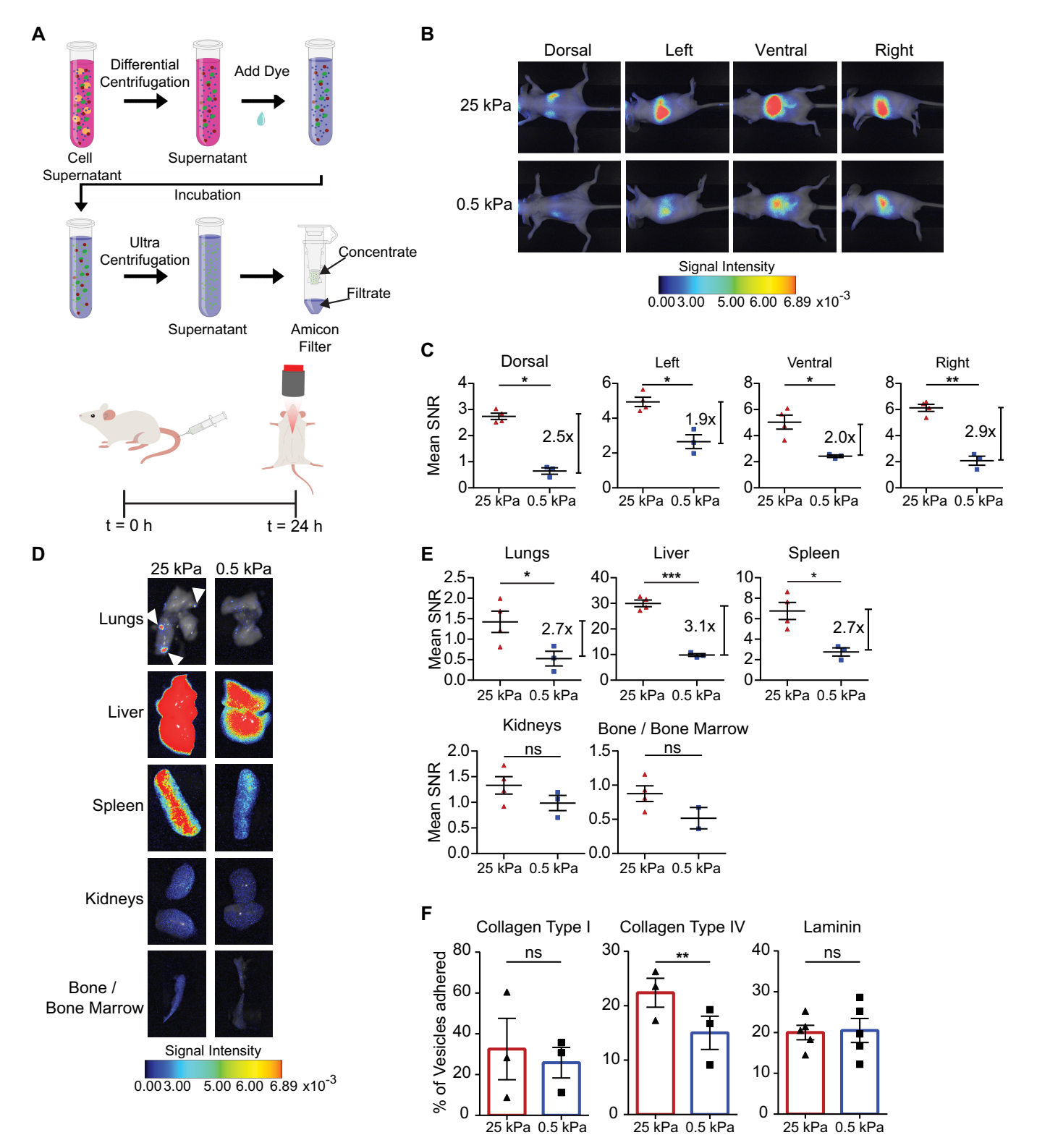
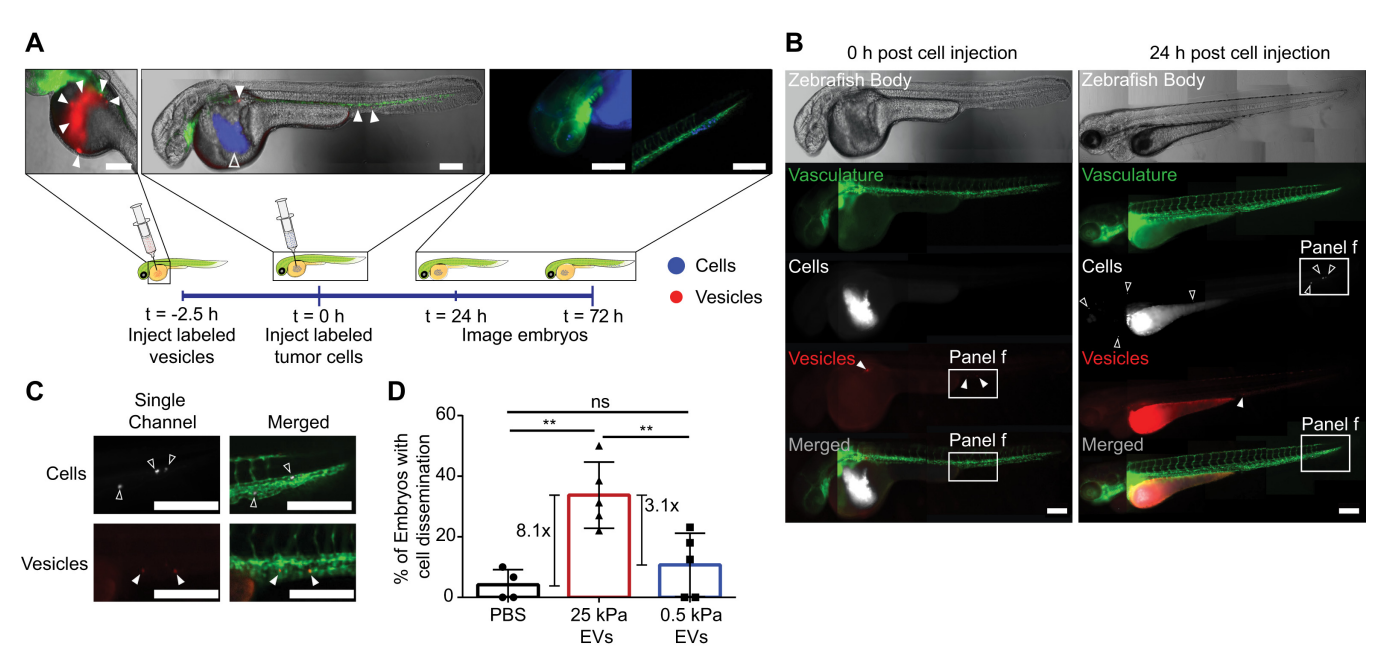


FIGURE 3 Stiff EVs show increased biodistribution and retention *in vivo*. **A,** Schematic of EV isolation and staining prior to tail-vein injection of 10 μg of EVs in nude mice. NIR imaging (**B**) and mean SNR (**C**) of MDA-MB-231 vesicle biodistribution in dorsal, left, ventral, and right sides (mean  $\pm$  SEM). Signal intensity is in arbitrary units (a.u.). Three mice in 0.5 kPa condition, and four in 25 kPa condition; one-way ANOVA. NIR imaging (**D**) and mean SNR biodistribution (**E**) in the lungs, liver, spleen, kidneys, and bone/bone marrow (mean  $\pm$  SEM). Signal intensity is in arbitrary units (a.u.). Three mice in MDA-MB-231 0.5 kPa condition and four in 25 kPa condition; one-way ANOVA. **F,** MDA-MB-231 EV binding assay to ECM proteins collagen type I, collagen type IV, and laminin (mean  $\pm$  SEM). Three biological repeats for collagen type I and collagen type IV; five for laminin. Paired *t* test.



**FIGURE 4** Stiff EVs promote cancer cell migration and dissemination. **A,** Schematic of 2-day GFP+ zebrafish embryo model system used to test the ability of MDA-MB-231 EVs (red, filled triangles) to disperse MDA-MB-231 cancer cells (blue, open triangles). Scale bar, 100 μm. **B,** Full zebrafish body images of the embryos at time 0 and 24 hours postinjection of MDA-MB-231 cancer cells. Scale bar, 100 μm. Representative images. **C,** Enlarged images of disseminated MDA-MB-231 cells (white) and EVs (red). Scale bar, 100 μm. Representative images. **D,** Percentage of injected embryos with cancer cell dissemination to the head or the tail. Total number of fish per condition is 47 for PBS control, 63 for 25 kPa, and 78 for 0.5 kPa condition. Five biological repeats of EVs. One-way ANOVA.

EVs significantly upregulated CAF-associated molecule (27, 88, 93–96) smooth muscle actin (*ACTA2*) 3.3-fold, connective tissue growth factor (*CCN2*) 1.5-fold, and vimentin (*VIM*) 2-fold relative to a vesicle-free condition (Fig. 5A). Interestingly, only matrix metalloproteinase 1 (*MMP1*) was upregulated by Stiff EVs (Fig. 5A). Instead, stiff EVs downregulated many of these CAF-associated genes including: *CCN2*, *IL6*, *KGF*, and *VIM* (Fig. 5A). While there was an approximately 10-fold increase in collagen type I expression from soft EVs, the difference was not significant (Fig. 5A). Comparatively, soft EVs had significantly higher ability to modulate *ACTA2*, *CCN2*, *IL6*, *KGF*, *VEGFA*, and *VIM* relative to stiff EVs.

We then probed how stiff and soft EVs regulated normal lung fibroblast gene expression of S100 proteins. In breast and pancreatic cancers, dysregulation of S100 protein expression, due in part to CAFs, is tied to an increase in growth, metastasis, and angiogenesis (98). Previously, the success of premetastatic niche formation in the lung was determined to be dependent on S100 protein upregulation (99). In lung fibroblasts exposed to soft EVs, we observed a noticeable upregulation of two S100 genes (S100A10 and S100A16; Fig. 5B) compared with a vesicle-free condition. Our results also indicate that stiff EVs downregulate the expression of S100A4, S100A6, S100A12, and S100A13. When compared with 0.5 kPa EVs, we observed a 6.8-fold (S100A4), 19.2-fold (S100A6), 3.8-fold (S100A12), and 4.3-fold (S100A13) decrease in expression (Fig. 5B). Together, these results suggest that soft vesicles produced by newly disseminated cancer cells in the soft microenvironment of the lung are significantly more effective at producing a CAF-like phenotype in lung fibroblasts via ensuing upregulation of S100 inflammatory signals and ACTA2//VEGFA/VIM (Fig. 5C).

## **Discussion**

This work demonstrates the importance of utilizing physiologically relevant conditions for studying the role of EVs in cancer. EVs released by cancer cells on plastic dishes differentially expressed hundreds of proteins, resulting in inaccurate information about the ability of vesicles to distribute *in vivo* and promote cell dissemination compared with matrices that mimic tissue stiffness at the primary and distant sites (Figs. 3 and 4). Our stiff tumor tissue and soft normal tissue matrices significantly altered EV quantity, protein cargo, function, and their potential to affect multiple aspects of the metastatic cascade.

The quantification of vesicles from primary patient breast tissue indicates that more EVs are released in stiff tissue over soft tissue. Within the tissue, there are many different cell types, all contributing to the number of small EVs we isolated in this study. As of now, there are no effective methods or markers for separating EVs based on the cell type of origin, which limits our ability to determine the number of vesicles produced by each cell type of the tumor microenvironment. We do notice though that there is an increase in cell number and density within the stiff breast tumor tissue compared with the soft breast tumor tissue (61). This result suggests increased cancer cell density may contribute to the observed EV secretion. Recent work done in hepatocellular carcinoma suggests this increased EV secretion on stiff environments is driven by activation of the Akt signaling pathway contributing to Rab8 mediated EV secretion (53).

In addition to the observed variations in stiffness-dependent vesicle secretion in breast cancer, the protein cargo of EVs critically depends on matrix stiffness. We identified a 3-fold increase in mean SNR between the stiff and soft EVs in

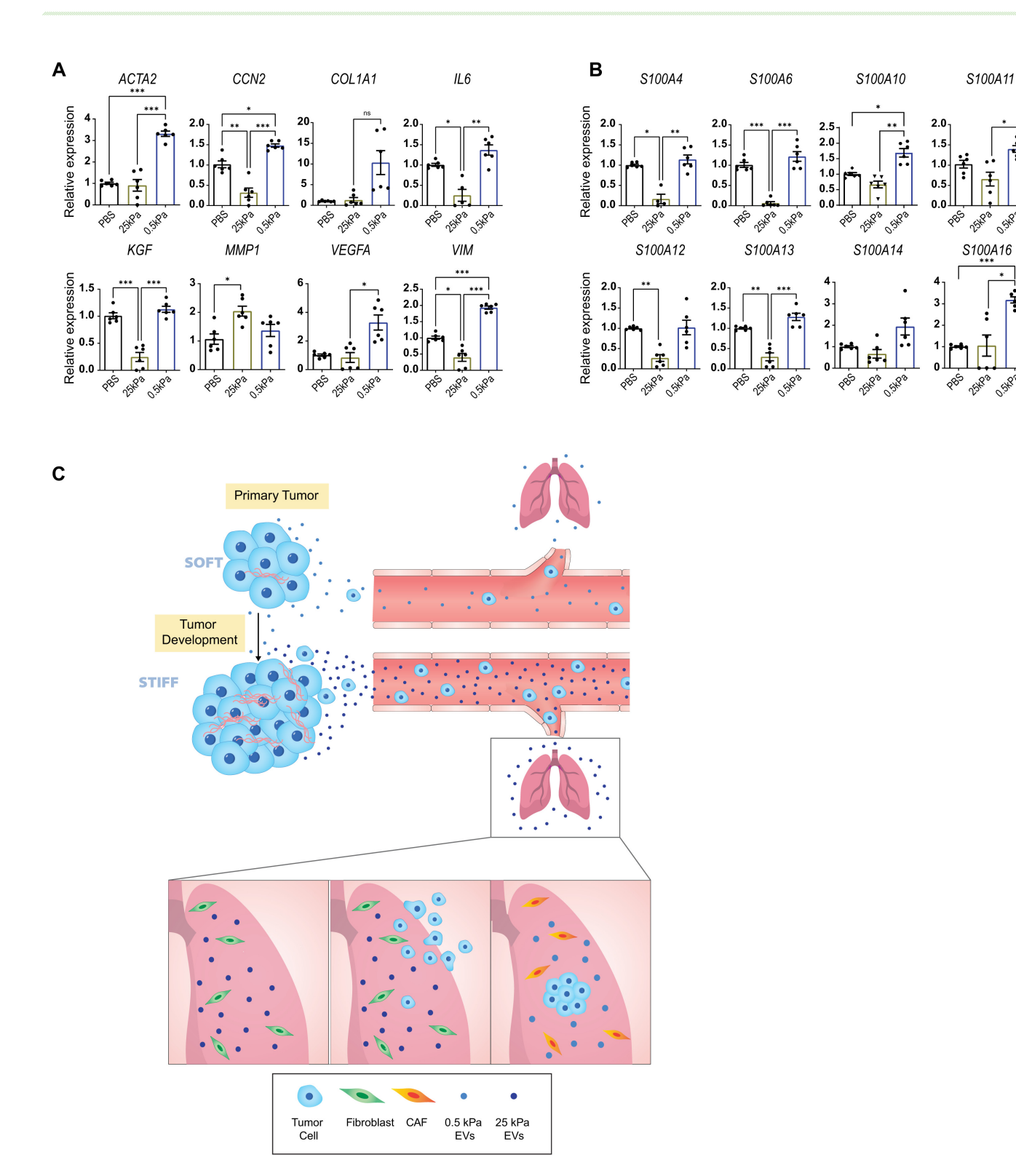


**FIGURE 5** Soft EVs transform the phenotype of resident lung fibroblasts. **A** and **B**, Gene expression fold change in *ACTA2*, *CCN2*, *COL1A1*, *IL6*, *KGF*, *MMP1*, *VIM*, *VEGFA*, *S100A4*, *S100A6*, *S100A10*, *S100A11*, *S100A12*, *S100A13*, *S100A14*, *S100A16* assessed by qRT-PCR in IMR90 human lung fibroblasts exposed to PBS only, 25 kPa EVs, and 0.5 kPa EVs. Gene expression data normalized to PBS condition. Two biological repeats. Welch ANOVA. **C**, Schematic showing the arrival of stiff EVs in the lung after being secreted from the primary tumor. Left panel shows a mechanically soft environment, and EVs encountering resident normal lung fibroblasts; (middle) cancer cells are then recruited to the lung; and (right) the cells, now experiencing a soft environment, release soft EVs that transform the resident fibroblasts to a CAF phenotype.

the lungs and liver, two of the most common sites of breast cancer metastasis. These results suggest that small EVs have a different rate of clearance in vivo as a function of stiffness, presumably due to our observed stiffness-dependent presentation of adhesion molecules on EVs and their ECM binding affinity (Fig 3F; Supplementary Fig. S2A). The increased retention of stiff EVs in the lung could be a function of specific integrins, including  $\alpha_6\beta_4$  and  $\alpha_6\beta_1$ , which have been previously linked to organotropic homing (48). Collagen type I, collagen type IV, and laminin have all been linked previously to cancer cell migration and invasion (80-82, 100-107). Collagen type IV lines all basement membranes in the liver and airway basement membrane in the lung (108, 109). Preferential binding of stiff EVs to basement-membrane proteins may, therefore, also explain increased stiff EV retention in the lungs and liver. Previously, small EVs were shown to increase lung vascular permeability in vivo (48). Our results suggest that stiff EVs, which bind these basement-membrane proteins promote cancer dissemination into the lung. This EV-mediated metastasis may be driven by thrombospondin-1 (THBSI) which overexpressed in stiff EVs (Supplementary Fig. S3B and S3C) was observed to regulate cancer cell motility (54). However, further studies are needed to delineate the mechanism driving soft EV retention in distal sites.

On the basis of zebrafish experiments, the mechanism driving EV-mediated cell movement is matrix dependent. Compared with soft EVs, stiff EVs demonstrated an enhanced ability to induce cancer dissemination *in vivo* (Fig. 4A–D). These findings in unison with EV proteomic data suggest that the proteins responsible for cell spreading from the primary tumor are preferentially sorted into EVs released by cancer cells experiencing a stiff tissue matrix.

While stiff EVs are more effective at promoting early step of the metastatic cascade through dissemination, we determined that stiff and soft EVs operate in a dynamic way to colonize distant organs, especially the lung. Once internalized by normal lung fibroblasts, the stiff EVs downregulate S100 expression, while soft EVs upregulate activation, vasculogenic, and inflammatory markers in the fibroblasts. The increased retention of stiff EVs in the lung and the downregulation of S100 proteins in normal resident lung fibroblasts may seem counterintuitive; however, a decrease in S100A4 expression has been linked to blocking fibroblast invasion and T-cell recruitment at the primary tumor (110). In addition, there is a direct relationship between the expressions of VEGFA and S100A4 in fibroblasts, with the expression of both molecules being important for metastatic colonization (111). Decreased S100A6 expression in breast cancer has been linked to a worse prognosis regardless of subtype (112). Although little has been studied about its role in breast cancer (112), S100A13 is known to regulate fibroblast growth factor (FGF1) and IL1α, which can affect the angiogenic and mitogenic properties of the tumor microenvironment (113-115). Therefore, the decrease in the expression of these S100 proteins in fibroblasts can promote a prometastatic environment in the lung, prior to the arrival of cancer cells. However, any functional changes observed in EV-modulated CAFs remain to

Once cancer cells arrive in the new soft environment of the lung, they release soft EVs that transform the resident fibroblasts toward a CAF phenotype through increased expression of *ACTA2*, *COLIAI*, and *VEGFA*, *VIM* (Fig. 5A). This interaction between soft environment and fibroblasts could also take place during early tumor progression or at other distant sites of metastasis (47, 64–69). The soft EVs demonstrate an upregulation of cytoskeletal regulating, binding, and cell signaling proteins linked to primary tumor growth (Fig. 5A).

and B). We propose that stiff EVs direct the recruitment of cancer cells and ensure retention in the lung by generating an anti-inflammatory environment; once there, the cancer cells experience a soft matrix and release soft EVs that transform the surrounding stroma to a protumorigenic environment. However, currently we are unable to delineate which cell types, if any, preferentially take up stiff and soft EVs. Further internalization studies are needed to understand EV cell type interactions.

Together our results indicate that EVs promote metastasis through multiple mechanisms that take advantage of the differences in stiffness of the primary and metastatic sites. The first is through the increased retention and biodistribution of stiff EVs in vivo, due to augmented binding to the ECM via increased integrin presentation, which allows for the formation of premetastatic niches. Second, EVs produced at both normal and tumor tissue stiffnesses affect changes to the surrounding ECM by regulating fibroblast activity. Stiff EVs decrease inflammatory signaling in the fibroblasts to facilitate cancer cell arrival at the lung, and once inside the mechanically soft lung, cancer cells release soft EVs that increase the expression of protumorigenic markers in the fibroblasts. Our findings highlight the critical importance of the physical properties of the ECM on the quantity, quality, and function of EVs produced by cancer cells in mediating their metastasis. Future exploration may focus on investigating pancancer markers of EV-driven stiffness-mediated metastasis for diagnostic and therapeutic applications.

## **Authors' Disclosures**

A. Sneider reports grants from National Science Foundation Graduate Research Fellowship during the conduct of the study. T.S. Eisinger-Mathason reports personal fees from Datavant outside the submitted work. No disclosures were reported by the other authors.

## **Authors' Contributions**

A. Sneider: Conceptualization, data curation, formal analysis, supervision, validation, investigation, visualization, methodology, writing-original draft, project administration. Y. Liu: Data curation, formal analysis, investigation, visualization, methodology, writing-original draft. B. Starich: Data curation, formal analysis, validation, investigation, visualization, methodology, writing-review and editing. W. Du: Data curation, formal analysis, validation, investigation, writing-review and editing. P.R. Nair: Supervision, validation, investigation, writing-review and editing. C. Marar: Investigation. N. Faqih: Investigation. G.E. Ciotti: Investigation. J.H. Kim: Investigation, methodology. S. Krishnan: Investigation, visualization. S. Ibrahim: Investigation. M. Igboko: Investigation, visualization. A. Locke: Investigation, visualization. D.M. Lewis: Investigation, visualization. H. Hong: Investigation. M.N. Karl: Investigation. R. Vij: Investigation. G.C. Russo: Investigation. E. Gómez-de-Mariscal: Data curation, formal analysis, investigation, visualization, methodology. M. Habibi: Resources. A. Muñoz-Barrutia: Resources, supervision, methodology. L. Gu: Resources, supervision, methodology. T.S.K. Eisinger-Mathason: Resources, supervision, methodology, writing-original draft, co-Corresponding Author. D. Wirtz: Conceptualization, resources, supervision, funding acquisition, visualization, methodology, writing-original draft, project administration, writing-review and editing.

# **Acknowledgments**

We would like to thank Dr. Simion Kremer and Dr. Bob Cole at the Mass Spectrometry and Proteomics Facility for the Johns Hopkins University School of Medicine for running the proteomics experiment and writing the Materials and Methods section. Thank you to Prof. Alan Meeker at the Johns Hopkins Oncology Tissue Services Core for his insight and guidance throughout the project. We thank Dr. Barbara Smith in the Kuo Microscopy Facility for taking TEM images and writing the corresponding methods section. We thank Vishnu Prasath, Dr. David Wilson, Prof. Jordan Green, Prof. Karen Reddy, Lindsay Rizzardi, Kimberly Stephens, the Sean Taverna Lab, the Andrew Feinberg Lab, Dr. Rada Cordero-Gonzalez, Prof. Arturo Casadevall, Josh DiGiacomo, and Prof. Daniele Gilkes for their expert help and access to resources for the project. We also thank Giulianna Leotta, Dr. Michael Harris, Prof. Ashley Kiemen, Dr. Meng Horn Lee, Prof. Pei-Hsun Wu, Dr. Adrian Johnston, Bailey Robertson, Prof. Jerry S.H. Lee (University of Southern California), Prof. Ken Witwer (Johns Hopkins University), and Prof. Martin Humphries (The University of Manchester) for fruitful discussions.

This work was supported by grants from the NCI (U54CA210173, U54CA143868, U54CA268083, R01CA174388), the National Institute on Aging (U01AG060903), and the National Institute of Arthritis and Musculoskeletal and Skin Diseases (U54AR081774) to D. Wirtz.; National Science Foundation Graduate Research Fellowship (1746891) to A. Sneider. In addition, the NVIDIA Corporation with the donation of the Titan X (Pascal) GPU (to A. Muñoz-Barrutia), Ministerio de Ciencia, Innovación y Universidades, Agencia Estatal de Investigación, under grants TEC2015-73064-EXP, TEC201678052-R and PID2019-109820RB-I00, MINECO/FEDER, UE, co-financed by European Regional Development Fund (ERDF), "A way of making Europe" (to A. Muñoz-Barrutia), and a 2017 Leonardo Grant for Researchers and Cultural Creators, BBVA Foundation (to A. Muñoz-Barrutia).

#### Note

Supplementary data for this article are available at Cancer Research Communications Online (https://aacrjournals.org/cancerrescommun/).

Received October 05, 2023; revised February 13, 2024; accepted April 15, 2024; published first May 09, 2024.

## References

- Van Der Rest M, Garrone R. Collagen family of proteins. FASEB J 1991;5: 2814-23.
- Frantz C, Stewart KM, Weaver VM. The extracellular matrix at a glance. J Cell Sci 2010:123: 4195-200.
- Rozario T, DeSimone DW. The extracellular matrix in development and morphogenesis: a dynamic view. Dev Biol 2010;341: 126-40.
- Naba A, Clauser KR, Hoersch S, Liu H, Carr SA, Hynes RO. The matrisome: in silico definition and in vivo characterization by proteomics of normal and tumor extracellular matrices. Mol Cell Proteomics 2012;11: M111.014647.
- Wells RG. The role of matrix stiffness in regulating cell behavior. Hepatology 2008:47: 1394-400.
- Wells RG. Tissue mechanics and fibrosis. Biochim Biophys Acta 2013;1832: 884-90.
- Cox TR, Erler JT. Remodeling and homeostasis of the extracellular matrix: implications for fibrotic diseases and cancer. Dis Model Mech 2011;4: 165-78.
- Handorf AM, Zhou Y, Halanski MA, Li W-J. Tissue stiffness dictates development, homeostasis, and disease progression. Organogenesis 2015;11: 1-15.
- 9. Colpaert C, Vermeulen P, Van Marck E, Dirix L. The presence of a fibrotic focus is an independent predictor of early metastasis in lymph node-negative breast cancer patients. Am J Surg Pathol 2001;25: 1557-8.
- Hasebe T, Tsuda H, Hirohashi S, Shimosato Y, Iwai M, Imoto S, et al. Fibrotic focus in invasive ductal carcinoma: an indicator of high tumor aggressiveness. Jpn J Cancer Res 1996;87: 385-94.
- Hasebe T, Tsuda H, Hirohashi S, Shimosato Y, Tsubono Y, Yamamoto H, et al. Fibrotic focus in infiltrating ductal carcinoma of the breast: a significant histopathological prognostic parameter for predicting the long-term survival of the patients. Breast Cancer Res Treat 1998;49: 195-208.
- Hasebe T, Sasaki S, Imoto S, Mukai K, Yokose T, Ochiai A, et al. Prognostic significance of fibrotic focus in invasive ductal carcinoma of the breast: a prospective observational study. Mod Pathol 2002;15: 502-16.
- Conklin MW, Eickhoff JC, Riching KM, Pehlke CA, Eliceiri KW, Provenzano PP, et al. Aligned collagen is a prognostic signature for survival in human breast carcinoma. Am J Pathol 2011;178: 1221-32.
- Drifka CR, Loeffler AG, Mathewson K, Keikhosravi A, Eickhoff JC, Liu Y, et al. Highly aligned stromal collagen is a negative prognostic factor following pancreatic ductal adenocarcinoma resection. Oncotarget 2016;7: 76197-213.

- Levental KR, Yu H, Kass L, Lakins JN, Egeblad M, Erler JT, et al. Matrix crosslinking forces tumor progression by enhancing integrin signaling. Cell 2009;139: 891-906
- Paszek MJ, Zahir N, Johnson KR, Lakins JN, Rozenberg GI, Gefen A, et al. Tensional homeostasis and the malignant phenotype. Cancer Cell 2005;8: 241-54
- Wei SC, Fattet L, Tsai JH, Guo Y, Pai VH, Majeski HE, et al. Matrix stiffness drives epithelial-mesenchymal transition and tumour metastasis through a TWIST1-G3BP2 mechanotransduction pathway. Nat Cell Biol 2015;17: 678-88.
- Rice AJ, Cortes E, Lachowski D, Cheung BCH, Karim SA, Morton JP, et al. Matrix stiffness induces epithelial-mesenchymal transition and promotes chemoresistance in pancreatic cancer cells. Oncogenesis 2017;6: e352.
- Sneider A, Cortes E, Lachowski D, Cheung BCH, Karim SA, Morton JP, et al. Deep learning identification of stiffness markers in breast cancer. Biomaterials 2022;285: 121540.
- Wynn TA, Ramalingam TR. Mechanisms of fibrosis: therapeutic translation for fibrotic disease. Nat Med 2012;18: 1028-40.
- 21. Wynn TA. Cellular and molecular mechanisms of fibrosis. J Pathol 2008;214: 199-210
- Chandler C, Liu T, Buckanovich R, Coffman LG. The double edge sword of fibrosis in cancer. Transl Res 2019;209: 55-67.
- Bordeleau F, Mason BN, Lollis EM, Mazzola M, Zanotelli MR, Somasegar S, et al. Matrix stiffening promotes a tumor vasculature phenotype. Proc Natl Acad Sci U S A 2017:114: 492-7.
- Reid SE, Kay EJ, Neilson LJ, Henze A-T, Serneels J, McGhee EJ, et al. Tumor matrix stiffness promotes metastatic cancer cell interaction with the endothelium. EMBO J 2017;36: 2373-89.
- Robins SP. Biochemistry and functional significance of collagen cross-linking. Biochem Soc Trans 2007;35: 849-52.
- Pankova D, Chen Y, Terajima M, Schliekelman MJ, Baird BN, Fahrenholtz M, et al. Cancer-associated fibroblasts induce a collagen cross-link switch in tumor stroma. Mol Cancer Res 2016;14: 287-95.
- 27. Kalluri R, Zeisberg M. Fibroblasts in cancer. Nat Rev Cancer 2006;6: 392-401.
- Tomasek JJ, Gabbiani G, Hinz B, Chaponnier C, Brown RA. Myofibroblasts and mechano: regulation of connective tissue remodelling. Nat Rev Mol Cell Biol 2002;3: 349-63.

- Langhans SA. Three-dimensional in vitro cell culture models in drug discovery and drug repositioning. Front Pharmacol 2018;9: 6.
- Lovitt C, Shelper T, Avery V. Advanced cell culture techniques for cancer drug discovery. Biology 2014;3: 345-67.
- Marar C, Starich B, Wirtz D. Extracellular vesicles in immunomodulation and tumor progression. Nat Immunol 2021;22: 560-70.
- 32. van Niel G, D'Angelo G, Raposo G. Shedding light on the cell biology of extracellular vesicles. Nat Rev Mol Cell Biol 2018;19: 213-28 .
- Doyle L, Wang M. Overview of extracellular vesicles, their origin, composition, purpose, and methods for exosome isolation and analysis. Cells 2019;8: 727.
- Wiklander OPB, Brennan M, Lötvall J, Breakefield XO, Andaloussi SEL. Advances in therapeutic applications of extracellular vesicles. Sci Transl Med 2019:11: eaav8521.
- 35. Veziroglu EM, Mias GI. Characterizing extracellular vesicles and their diverse RNA contents. Front Genet 2020;11: 700.
- Arenaccio C, Federico M. The multifaceted functions of exosomes in health and disease: an overview. Adv Exp Med Biol 2017;998: 3-19.
- Kowal J, Arras G, Colombo M, Jouve M, Morath JP, Primdal-Bengtson B, et al. Proteomic comparison defines novel markers to characterize heterogeneous populations of extracellular vesicle subtypes. Proc Natl Acad Sci U S A 2016;113: E968-77.
- Zaborowski MP, Balaj L, Breakefield XO, Lai CP. Extracellular vesicles: composition, biological relevance, and methods of study. Bioscience 2015;65: 783-97.
- Wiklander OP, Nordin JZ, O'Loughlin A, Gustafsson Y, Corso G, Mäger I, et al. Extracellular vesicle *in vivo* biodistribution is determined by cell source, route of administration and targeting. J Extracell Vesicles 2015;4: 26316.
- Corrado C, Raimondo S, Chiesi A, Ciccia F, De Leo G, Alessandro R, et al. Exosomes as intercellular signaling organelles involved in health and disease: basic science and clinical applications. Int J Mol Sci 2013;14: 5338-66.
- Isola A, Chen S. Exosomes: the messengers of health and disease. Curr Neuropharmacol 2016;15: 157-65.
- Montecalvo A, Larregina AT, Shufesky WJ, Stolz DB, Sullivan MLG, Karlsson JM, et al. Mechanism of transfer of functional microRNAs between mouse dendritic cells via exosomes. Blood 2012;119: 756-66.
- Segura E, Guérin C, Hogg N, Amigorena S, Théry C. CD8 + dendritic cells use LFA-1 to capture MHC-peptide complexes from exosomes in vivo. J Immunol 2007;179: 1489-96.
- Segura E, Amigorena S, Théry C. Mature dendritic cells secrete exosomes with strong ability to induce antigen-specific effector immune responses. Blood Cells Mol Dis 2005;35: 89-93.
- Raposo G, Nijman HW, Stoorvogel W, Liejendekker R, Harding CV, Melief CJ, et al. B lymphocytes secrete antigen-presenting vesicles. J Exp Med 1996;183: 1161-72.
- Luga V, Zhang L, Viloria-Petit AM, Ogunjimi AA, Inanlou MR, Chiu E, et al. Exosomes mediate stromal mobilization of autocrine Wnt-PCP signaling in breast cancer cell migration. Cell 2012;151: 1542-56.
- Peinado H, Aleckovic M, Lavotshkin S, Matei I, Costa-Silva B, Moreno-Bueno G, et al. Melanoma exosomes educate bone marrow progenitor cells toward a pro-metastatic phenotype through MET. Nat Med 2012;18: 883-91.
- Hoshino A, Costa-Silva B, Shen T-L, Rodrigues G, Hashimoto A, Mark MT, et al. Tumour exosome integrins determine organotropic metastasis. Nature 2015;527: 329-35.
- Costa-Silva B, Aiello NM, Ocean AJ, Singh S, Zhang H, Thakur BK, et al. Pancreatic cancer exosomes initiate pre-metastatic niche formation in the liver. Nat Cell Biol 2015:17: 816-26.
- Peinado H, Zhang H, Matei IR, Costa-Silva B, Hoshino A, Rodrigues G, et al. Pre-metastatic niches: organ-specific homes for metastases. Nat Rev Cancer 2017;17: 302-17.
- Parolini I, Federici C, Raggi C, Lugini L, Palleschi S, De Milito A, et al. Microenvironmental pH is a key factor for exosome traffic in tumor cells. J Biol Chem 2009:284: 34211-22.
- Clayton A, Mitchell JP, Court J, Linnane S, Mason MD, Tabi Z, et al. Human tumor-derived exosomes down-modulate NKG2D expression. J Immunol 2008;180: 7249-58.

- Wu B, Liu DA, Guan L, Myint PK, Chin L, Dang H, et al. Stiff matrix induces exosome secretion to promote tumour growth. Nat Cell Biol 2023;25: 415-24
- Patwardhan S, Mahadik P, Shetty O, Sen S. ECM stiffness-tuned exosomes drive breast cancer motility through thrombospondin-1. Biomaterials 2021;279: 121185.
- Giri A, Bajpai S, Trenton N, Jayatilaka H, Longmore GD, Wirtz D. The Arp2/3 complex mediates multigeneration dendritic protrusions for efficient 3-dimensional cancer cell migration. FASEB J 2013;27: 4089-99.
- Nair PR, Danilova L, Gómez-de-Mariscal E, Kim D, Fan R, Muñoz-Barrutia A, et al. MLL1 regulates cytokine-driven cell migration and metastasis. Sci Adv 2024:10: eadk0785.
- Akhtar R, Draper ER, Adams DJ, Hay J. Oscillatory nanoindentation of highly compliant hydrogels: a critical comparative analysis with rheometry. J Mater Res 2018:33: 873-83.
- 58. Sneddon IN. The relation between load and penetration in the axisymmetric boussinesg problem for a punch of arbitrary profile. Int J Eng Sci 1965;3: 47-57.
- Herbert EG, Oliver WC, Lumsdaine A, Pharr GM. Measuring the constitutive behavior of viscoelastic solids in the time and frequency domain using flat punch nanoindentation. J Mater Res 2009;24: 626-37.
- Herbert EG, Oliver WC, Pharr GM. Nanoindentation and the dynamic characterization of viscoelastic solids. J Phys D Appl Phys 2008;41: 074021.
- Sneider A, Kiemen A, Kim JH, Wu P-H, Habibi M, White M, et al. Deep learning identification of stiffness markers in breast cancer. Biomaterials 2020;285: 121540.
- Grifno GN, Farrell AM, Linville RM, Arevalo D, Kim J, Gu L, et al. Tissueengineered blood-brain barrier models via directed differentiation of human induced pluripotent stem cells. Sci Rep 2019;9: 13957.
- Bligh EG, Dyer WJ. A rapid method of total lipid extraction and purification. Can J Biochem Physiol 1959;37: 911-7.
- Diel IJ, Goerner R, Costa SD, Kaul S, Bastert G. Detection of tumor cells in bone marrow of patients with primary breast cancer: a prognostic factor for distant metastasis. J Clin Oncol 1992;10: 1534-9.
- 65. Shiozawa Y, Eber MR, Berry JE, Taichman RS. Bone marrow as a metastatic niche for disseminated tumor cells from solid tumors. Bonekey Rep 2015;4: 689
- Lindemann F, Witte J, Schlimok G, Dirschedl P, Riethmuller G. Prognostic significance of micrometastatic tumour cells in bone marrow of colorectal cancer patients. Lancet 1992:340: 685-9.
- Pantel K, Izbicki J, Passlick B, Angstwurm M, Häussinger K, Thetter O, et al. Frequency and prognostic significance of isolated tumour cells in bone marrow of patients with non-small-cell lung cancer without overt metastases. Lancet 1996;347: 649-53.
- 68. Janmey PA, Miller RT. Mechanisms of mechanical signaling in development and disease. J Cell Sci 2011;124: 9-18.
- Griesenauer RH, Weis JA, Arlinghaus LR, Meszoely IM, Miga MI. Breast tissue stiffness estimation for surgical guidance using gravity-induced excitation. Phys Med Biol 2017;62: 4756-76.
- Syed S, Schober J, Blanco A, Zustiak SP. Morphological adaptations in breast cancer cells as a function of prolonged passaging on compliant substrates. PLoS One 2017:12: e0187853.
- Raposo G, Stoorvogel W. Extracellular vesicles: exosomes, microvesicles, and friends. J Cell Biol 2013;200: 373-83.
- Rikkert LG, Nieuwland R, Terstappen LWMM, Coumans FAW. Quality of extracellular vesicle images by transmission electron microscopy is operator and protocol dependent. J Extracell Vesicles 2018;8: 1555419.
- Gómez-de-Mariscal E, Maška M, Kotrbová A, Pospíchalová V, Matula P, Muñoz-Barrutia A, et al. Deep-learning-based segmentation of small extracellular vesicles in transmission electron microscopy images. Sci Rep 2019;9: 17211
- Théry C, Witwer KW, Aikawa E, Alcaraz MJ, Anderson JD, Andriantsitohaina R, et al. Minimal information for studies of extracellular vesicles 2018 (MI-SEV2018): a position statement of the International Society for Extracellular Vesicles and update of the MISEV2014 guidelines. J Extracell Vesicles 2018;7: 1535750

- Stopa KB, Kusiak AA, Szopa MD, Ferdek PE, Jakubowska MA. Pancreatic cancer and its microenvironment—recent advances and current controversies. Int J Mol Sci 2020:21: 3218.
- Nabavizadeh A, Payen T, luga AC, Sagalovskiy IR, Desrouilleres D, Saharkhiz N, et al. Noninvasive Young's modulus visualization of fibrosis progression and delineation of pancreatic ductal adenocarcinoma (PDAC) tumors using Harmonic Motion Elastography (HME) in vivo. Theranostics 2020;10: 4614-26.
- 77. Weniger M, Honselmann KC, Liss AS. The extracellular matrix and pancreatic cancer: a complex relationship. Cancers 2018;10: 316.
- Rubiano A, Delitto D, Han S, Gerber M, Galitz C, Trevino J, et al. Viscoelastic properties of human pancreatic tumors and in vitro constructs to mimic mechanical properties. Acta Biomater 2018;67: 331-40.
- Zhou Y, Zhou B, Pache L, Chang M, Khodabakhshi AH, Tanaseichuk O, et al. Metascape provides a biologist-oriented resource for the analysis of systems-level datasets. Nat Commun 2019:10: 1523.
- Ioachim E, Charchanti A, Briasoulis E, Karavasilis V, Tsanou H, Arvanitis DL, et al. Immunohistochemical expression of extracellular matrix components tenascin, fibronectin, collagen type IV and laminin in breast cancer: their prognostic value and role in tumour invasion and progression. Eur J Cancer 2002;38: 2362-70.
- 81. Hewitt R, Powe DG, Morrell K, Balley E, Leach IH, et al. Laminin and collagen IV subunit distribution in normal and neoplastic tissues of colorectum and breast. Br J Cancer 1997;75: 221-9.
- 82. Khoshnoodi J, Pedchenko V, Hudson BG. Mammalian collagen IV. Microsc Res Tech 2008;71: 357-70.
- Ishii S, Ford R, Thomas P, Nachman A, Steele G Jr, Jessup JM. CD44 participates in the adhesion of human colorectal carcinoma cells to laminin and type IV collagen. Surg Oncol 1993;2: 255-64.
- 84. Lauer-Fields JL, Malkar NB, Richet G, Drauz K, Fields GB. Melanoma cell CD44 interaction with the  $\alpha$ 1(IV)1263–1277 region from basement membrane collagen is modulated by ligand glycosylation. J Biol Chem 2003;278: 14321-30.
- 85. Kleiser S, Nyström A. Interplay between cell-surface receptors and extracellular matrix in skin. Biomolecules 2020;10: 1170.
- 86. Meyer T, Marshall JF, Hart IR. Expression of alphav integrins and vitronectin receptor identity in breast cancer cells. Br J Cancer 1998;77: 530-6.
- 87. Miroshnikova YA, Rozenberg GI, Cassereau L, Pickup M, Mouw JK, Ou G, et al.  $\alpha$ 5 $\beta$ 1-Integrin promotes tension-dependent mammary epithelial cell invasion by engaging the fibronectin synergy site. Mol Biol Cell 2017;28: 2958-77.
- 88. Bhowmick NA, Neilson EG, Moses HL. Stromal fibroblasts in cancer initiation and progression. Nature 2004;432: 332-7.
- 89. McAnulty RJ. Fibroblasts and myofibroblasts: their source, function and role in disease. Int J Biochem Cell Biol 2007;39: 666-71.
- Smith RS, Smith TJ, Blieden TM, Phipps RP. Fibroblasts as sentinel cells. Synthesis of chemokines and regulation of inflammation. Am J Pathol 1997;151: 317-22.
- 91. Hinz B. Mechanical aspects of lung fibrosis. Proc Am Thorac Soc 2012;9: 137-47.
- Polio SR, Kundu AN, Dougan CE, Birch NP, Aurian-Blajeni DE, Schiffman JD, et al. Cross-platform mechanical characterization of lung tissue. PLoS One 2018;13: e0204765.
- Chen Y, Abraham DJ, Shi-Wen X, Pearson JD, Black CM, Lyons KM, et al. CCN2 (connective tissue growth factor) promotes fibroblast adhesion to fibronectin. Mol Biol Cell 2004;15: 5635-46.
- 94. Sundararaj KP, Samuvel DJ, Li Y, Sanders JJ, Lopes-Virella MF, Huang Y. Interleukin-6 released from fibroblasts is essential for up-regulation of matrix metalloproteinase-1 expression by U937 macrophages in coculture: crosstalking between fibroblasts and U937 macrophages exposed to high glucose. J Biol Chem 2009;284: 13714-24.

- Salgado R, Junius S, Benoy I, Dam PV, Vermeulen P, Marck EV, et al. Circulating interleukin-6 predicts survival in patients with metastatic breast cancer. Int J Cancer 2003:103: 642-6.
- DeMichele A, Martin AM, Mick R, Gor P, Wray L, Klein-Cabral M, et al. Interleukin-6 -174G->C polymorphism is associated with improved outcome in high-risk breast cancer. Cancer Res 2003;63: 8051-6.
- Ronnov-Jessen L, Petersen OW, Bissell MJ. Cellular changes involved in conversion of normal to malignant breast: importance of the stromal reaction. Physiol Rev 1996;76: 69-1152
- 98. Bresnick AR, Weber DJ, Zimmer DB. S100 proteins in cancer. Nat Rev Cancer 2015:15: 96-109.
- Kaplan RN, Riba RD, Zacharoulis S, Bramley AH, Vincent L, Costa C, et al. VEGFR1-positive haematopoietic bone marrow progenitors initiate the pre-metastatic niche. Nature 2005;438: 820-7.
- Hamill KJ, Kligys K, Hopkinson SB, Jones JCR. Laminin deposition in the extracellular matrix: a complex picture emerges. J Cell Sci 2009;122: 4409-17.
- Hurt EM, Chan K, Duhagon Serrat MA, Thomas SB, Veenstra TD, Farrar WL, et al. Identification of vitronectin as an extrinsic inducer of cancer stem cell differentiation and tumor formation. Stem Cells 2009;28: 390-8.
- 102. Kadowaki M, Sangai T, Nagashima T, Sakakibara M, Yoshitomi H, Takano S, et al. Identification of vitronectin as a novel serum marker for early breast cancer detection using a new proteomic approach. J Cancer Res Clin Oncol 2011;137: 1105-15.
- 103. Mcdonald JA. Extracellular matrix assembly. Ann Rev Cell Bioi 1988;4: 183-207.
- 104. George EL, Georges-Labouesse EN, Patel-King RS, Rayburn H, Hynes RO. Defects in mesoderm, neural tube and vascular development in mouse embryos lacking fibronectin. Development 1993;119: 1079-91.
- 105. Jensen BV, Johansen JS, Skovsgaard T, Brandt J, Teisner B. Extracellular matrix building marked by the N-terminal propeptide of procollagen type I reflect aggressiveness of recurrent breast cancer. Int J Cancer 2002;98: 582-9.
- Provenzano PP, Inman DR, Eliceiri KW, Knittel JG, Yan L, Rueden CT, et al. Collagen density promotes mammary tumor initiation and progression. BMC Med 2008;6: 11.
- 107. Gilkes DM, Semenza GL, Wirtz D. Hypoxia and the extracellular matrix: drivers of tumour metastasis. Nat Rev Cancer 2014;14: 430-9.
- Roche WR, Williams JH, Beasley R, Holgate ST. Subepithelial fibrosis in the bronchi of asthmatics. Lancet 1989:333: 520-4.
- Rosmark O, Åhrman E, Müller C, Rendin LE, Eriksson L, Malmström A, et al. Quantifying extracellular matrix turnover in human lung scaffold cultures. Sci Rep 2018;8: 5409.
- Klingelhöfer J, Grum-Schwensen B, Beck MK, Petersen Knudsen RS, Grigorian M, Lukanidin E, et al. Anti-S100A4 antibody suppresses metastasis formation by blocking stroma cell invasion. Neoplasia 2012;14: 1260-8.
- O'Connell JT, Sugimoto H, Cooke VG, MacDonald BA, Mehta AI, LeBleu VS, et al. VEGF-A and Tenascin-C produced by S100A4+ stromal cells are important for metastatic colonization. Proc Natl Acad Sci U S A 2011;108: 16002-7.
- 112. Zhang S, Wang Z, Liu W, Lei R, Shan J, Li L, et al. Distinct prognostic values of S100 mRNA expression in breast cancer. Sci Rep 2017;7: 39786.
- 113. Rani SG, Mohan SK, Yu C. Molecular level interactions of S100A13 with amlexanox: inhibitor for formation of the multiprotein complex in the nonclassical pathway of acidic fibroblast growth factor. Biochemistry 2010;49: 2585-92.
- 114. Prudovsky I, Mandinova A, Soldi R, Bagala C, Graziani I, Landriscina M, et al. The non-classical export routes: FGF1 and IL-1α point the way. J Cell Sci 2003;116: 4871-81
- Landriscina M, Schinzari G, Di Leonardo G, Quirino M, Cassano A, D'Argento E, et al. S100A13, a new marker of angiogenesis in human astrocytic gliomas. J Neurooncol 2006:80: 251-9.